A novel Kriging-assisted multi-objective optimization method considering infeasibility ratio under input uncertainty

Hua Wei[a]*, Qi Zhou[b], Tom Dhaene[a], Ivo Couckuyt[a]

[a]*Department of Information Technology (INTEC), IDLab, Ghent University-imec, Ghent, 9052, Belgium;* [b]*School of Aerospace Engineering, Huazhong University of Science and Technology, Wuhan, 430074, China*

Email address: hua.wei@ugent.be

A novel Kriging-assisted multi-objective optimization method considering infeasibility ratio under input uncertainty

Many real-life engineering applications come with various sources of uncertainty. Uncertainty can also impact the feasibility of solutions in constrained optimization. Classic robust optimization approaches often significantly increase the computational burden and might overlook different tolerable risks, resulting in conservative sub-optimal solutions. We reformulate the classic constrained problem as a multi-objective optimization problem and propose a Kriging-assisted multi-objective optimization method that trades off Infeasibility Ratio (IR) with robust performance: (1) a formulation to approximate IR is developed and introduced as an additional objective and (2) an acquisition function balancing exploration (refining feasible boundaries) and exploitation of promising areas with multiple designs is proposed. Furthermore, a new quality metric has been developed to effectively measure the convergence and diversity of the obtained Pareto solution set. The proposed framework is tested on five numerical problems and applied to an engineering case: the design of a honeycomb vibration isolator. A comparison study with other optimization methods is conducted to verify its effectiveness and performance with promising results.

Keywords: multi-objective optimization; constraint handling strategy; sequential sampling; input uncertainty; Kriging model

1. Introduction

Real-life engineering design problems are usually multi-objective, subject to restrictive constraints, with uncertainties in design variables or parameters, and require expensive physical or simulation experiments (Gunantara 2018; He et al. 2023; Li et al. 2023; Long et al. 2023; Kudva, Tang, and Paulson 2023). Dealing with uncertainty is a tricky issue when designing complex modern engineering systems (Qing, Couckuyt, and Dhaene 2023; Zhang and Taflanidis 2019; Li et al. 2022; Juul-Nyholm and Eifler 2023; Kudva, Tang, and Paulson 2023). These uncertainties, such as the manufacturing uncertainty or geometric errors of machine parts, may impair the performance stability of mechanical systems, decrease the service life, or even result in infeasible design solutions (Xie et al.

2018; Kania and Azarm 2023a; Lin et al. 2022). Additionally, the expensive physical experiment or time-consuming simulation makes the optimization design of practical engineering applications more challenging (Lin et al. 2023; Qian et al. 2021; Loka et al. 2023).

The population-based multi-objective evolution algorithms (MOEA) have been widely studied due to their ability to solve complex and intractable multi-objective optimization (MOO) problems (Jin et al. 2018). However, the time-consuming simulations make it impractical for MOEAs (Zhou et al. 2021). A popular approach is to use surrogate models trained on a limited number of evaluations (Kania and Azarm 2023b; Zhou and Ren 2025). For example, Song et al. (2021) proposed an efficient Kriging-assisted MOEA with an active sampling strategy to guide the infill process balancing convergence, diversity, and model uncertainty. Besides, many real-life optimization problems may be subjected to strict constraints (Dang et al. 2025). Various constraint-handling strategies (CHS), such as penalty-based methods and constraint dominance principle-based methods (Ma and Wang 2021; Deb et al. 2002), are employed to assist MOEAs (Li et al. 2023). Roy et al. (2021) proposed a constrained MOO method assisted by Radial Basis Function approximations as surrogates for objectives and constraints. Song et al. (2023) proposed a switching strategy to balance objective optimization and constraint satisfaction when solving expensive constrained optimization problems. In addition to surrogate-assisted MOEAs, the Efficient Global Optimization (EGO) framework has attracted considerable research interest (Liu, Grout, and Nikolaeva 2017; Jones, Schonlau, and Welch 1998; Price and Robertson 2024) due to its high efficiency. However, the research that considers the negative influence of input uncertainties on the performance and feasibility during the design process is limited.

Numerous robust strategies have been investigated in the literature to support

MOO methods in handling input uncertainty during optimization. Wauters (2024) proposed a robust global MOO method that incorporates failed function evaluations to guarantee the feasibility and robustness of the obtained solution set. Xie et al. (2018) adopted a Support Vector Machine classifier to represent the constraints. In Wei et al. (2024), the probability of feasibility is used to locate feasible regions that are less sensitive to input uncertainty. Most constrained robust MOO methods, such as the worst-case scenario evaluation, adopt a binary judgment when evaluating the feasibility under input uncertainty (Kania and Azarm 2023b). However, in engineering, it is often practical to trade off performance for high confidence level of feasibility and vice versa (Song et al. 2024; Chaudhuri, Marques, and Willcox 2021; Zhong et al. 2022).

The typical binary classification ignores the varying degrees to which design solutions are affected by input uncertainty. This limitation may result in MOO algorithms being too conservative to fully exploit the potential design space and obtain diverse promising solutions (Wei et al. 2021). Therefore, an Infeasibility Ratio (IR) formulation is proposed to approximate the possibility of infeasibility for each intermediate candidate when input uncertainty makes the constraint responses fluctuate. To guarantee the accuracy of the IR approximation, the surrogate model should be able to provide an accurate prediction of the constraint limit state. Representatively, the Expected Feasibility (EF) function (Yi et al. 2021) demonstrates a strong ability to explore constraint boundaries. By maximizing the EF function, the algorithm iteratively updates the sample set for the surrogate model to refine the prediction of the feasible boundary (Bichon et al. 2008). However, it struggles to effectively balance constraint boundary exploration and objective optimization with different IR levels.

In this work, a new Kriging-assisted Multi-objective Optimization method considering the Infeasibility Ratio under input uncertainty (KMO-IR) is developed to

address the limitations of MOO methods using binary classification as CHS. The main novelties and contributions include: (a) the KMO-IR method adopts the IR formulation to evaluate the possibility of being infeasible for a solution without extra computational effort; (b) by simultaneously optimizing the design performance and the IR, the algorithm can obtain Pareto solutions with different levels of feasibility; (c) a new acquisition function combining a quality index of Pareto Front (PF) is proposed to iteratively search for the most promising candidate; (d) a comparative experiment is conducted between the KMO-IR method and four existing optimization methods on five numerical benchmark functions; (e) the constrained optimization design of a metamaterial vibration isolator with a honeycomb structure is solved and a comparative analysis illustrating the competitiveness and advantages of the KMO-IR method is completed.

The backgrounds related to this work are explained in Section 2. Section 3 elaborates on the detailed methodology of the proposed KMO-IR method. The comparison results of numerical experiments and the engineering application are presented in Section 4 and Section 5, respectively. Section 6 provides the conclusions.

2. Background

2.1. Constrained Multi-Objective Optimization

A general expression of constrained MOO problem with M objective functions is given as

$$\begin{aligned} &\min_{\boldsymbol{x}} \ \boldsymbol{f}(\boldsymbol{x})=\left\{f_1(\boldsymbol{x}), f_2(\boldsymbol{x}),..., f_M(\boldsymbol{x})\right\} \\ &\text{s.t. } \ \boldsymbol{x}\in[\boldsymbol{x}^{\mathrm{LB}}, \boldsymbol{x}^{\mathrm{UB}}] \\ &\boldsymbol{g}(\boldsymbol{x})=\max(g_1(\boldsymbol{x}),g_2(\boldsymbol{x}),..., g_J(\boldsymbol{x}),0)\le 0 \end{aligned} \tag{1}$$

$[\boldsymbol{x}^{\mathrm{LB}}, \boldsymbol{x}^{\mathrm{UB}}]$ represents the design space. $\boldsymbol{g}(\boldsymbol{x})$ includes J constraint functions. The goal of MOO is to obtain Pareto set in design space, corresponding to the PF in output space. In a PF, the improvement of one objective is accompanied by the other's sacrificing.

Many metrics are used to measure the quality of the PF, such as the Hyper Area Difference (HAD), Inverted Generational Distance (IGD), Average Hyper Area (AHA), and Overall Spread (OS)(Jin et al. 2019; Wu and Azarm 2001; Cheng, Zhou, and Li 2015). The HAD and IGD require the real PF, which is usually intractable in real engineering applications, while the AHA is inadequate for quantifying the refinement and extension of an observed PF (Shu et al. 2020). The OS works effectively only if all PFs are converged to the true PF; otherwise, a larger value is meaningless. Shu et al. (2020) proposed the modified Hyper Area (mHA), which overcomes the shortcomings of AHA's inability to assess refinement. The illustration of mHA is shown in Figure 1(a). Figure 1(b) provides a schematic representation of OS.

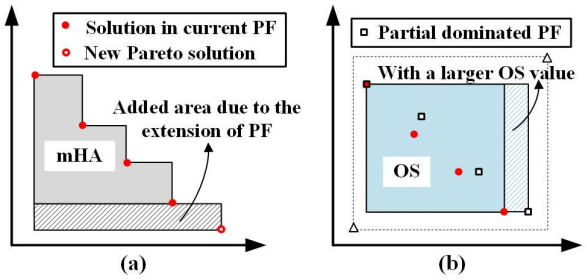

Figure 1. The schematic representations of (a) modified Hyper Area (mHA) and (b) Overall Spread (OS) in a two-objective case. The two triangles in (b) are reference points, corresponding to the all-best and all-worst cases, respectively.

2.2. Efficient Robust Global Optimisation (ERGO)

The ERGO algorithm to handles input uncertainty when optimizing objective performance (Wauters 2022). There are two stages included: the initial Kriging model construction (Appendix 1 for more details); and the sequential selection strategy, i.e. Expected Improvement (EI), which is defined as

$$EI(\boldsymbol{x}) = \begin{cases} I(\boldsymbol{x}) \cdot \Phi\left(\frac{I(\boldsymbol{x})}{\hat{e}(\boldsymbol{x})}\right) + \hat{e}(\boldsymbol{x}) \cdot \phi\left(\frac{I(\boldsymbol{x})}{\hat{e}(\boldsymbol{x})}\right), \hat{e}(\boldsymbol{x}) > 0 \\ 0, \hat{e}(\boldsymbol{x}) = 0 \end{cases} . \quad (2)$$

$$where \quad I(\boldsymbol{x}) = \min(\boldsymbol{Y}) - \hat{y}(\boldsymbol{x})$$

$\hat{y}(\boldsymbol{x})$ and $\hat{e}^2(\boldsymbol{x})$ are the mean and variance predicted by the Kriging model of the unobserved point $\boldsymbol{x}$. The Φ and ϕ are the cumulative distribution and probability distribution functions of normal distribution, respectively.

When input uncertainty is considered during the optimization process, the output objective is stochastic. Wauters (2022) formed a second-order Taylor-based uncertainty propagation (UP) approach through a Kriging, which considers both the model error and input perturbations. The Robust Expected Improvement (REI), given in Eq. (3), is proposed in ERGO to simultaneously optimize $E\left[y(\tilde{\boldsymbol{x}})\right]$ and $V\left[y(\tilde{\boldsymbol{x}})\right]$, indicating the expected value of the objective and the corresponding variance caused by input uncertainty, respectively.

$$
\begin{aligned}
&REI\left(\tilde{\boldsymbol{x}}\right) = P[RI\left(\tilde{\boldsymbol{x}}\right)]\cdot\left[Eud(\tilde{\boldsymbol{x}},\boldsymbol{X}^*)\right]_{\min} \\
&\text{where} \\
&Eud(\tilde{\boldsymbol{x}},\boldsymbol{X}^*) = \sqrt{\begin{aligned}&(E(y(\boldsymbol{X}^*)) - E(y(\tilde{\boldsymbol{x}})))^2 \\ &+(V(y(\boldsymbol{X}^*)) - V(y(\tilde{\boldsymbol{x}})))^2\end{aligned}}
\end{aligned}
\tag{3}
$$

$\boldsymbol{X}^*$ is the current optimal solution set while $\tilde{\boldsymbol{x}}$ indicates the potential design with input uncertainty. $P[RI\left(\tilde{\boldsymbol{x}}\right)]$ represents the probability of improvement. More detailed information can be found in (Wauters 2022).

In this work, the UP-based Kriging from ERGO is adopted to provide the variance caused by input uncertainty, which is essential for the IR formulation.

2.3. Expected Feasibility

The EF function (Bichon et al. 2008) is used to refine the boundary ($g_j(\boldsymbol{x}_{\text{un}})=0$) of the feasible region instead of only focusing on exploring the inside of the feasible region. Its expression is given as

$$
\begin{aligned}
EF\left(\hat{g}_j(\boldsymbol{x}_{\text{un}})\right) = \hat{g}_j(\boldsymbol{x}_{\text{un}})[2\Phi(\frac{-\hat{g}_j(\boldsymbol{x}_{\text{un}})}{e_j(\boldsymbol{x}_{\text{un}})}) - \Phi(\frac{-\varepsilon-\hat{g}_j(\boldsymbol{x}_{\text{un}})}{e_j(\boldsymbol{x}_{\text{un}})}) - \Phi(\frac{+\varepsilon-\hat{g}_j(\boldsymbol{x}_{\text{un}})}{e_j(\boldsymbol{x}_{\text{un}})})] \\
- e_j(\boldsymbol{x}_{\text{un}})[2\phi(\frac{-\hat{g}_j(\boldsymbol{x}_{\text{un}})}{e_j(\boldsymbol{x}_{\text{un}})}) - \phi(\frac{-\varepsilon-\hat{g}_j(\boldsymbol{x}_{\text{un}})}{e_j(\boldsymbol{x}_{\text{un}})}) - \phi(\frac{+\varepsilon-\hat{g}_j(\boldsymbol{x}_{\text{un}})}{e_j(\boldsymbol{x}_{\text{un}})})] \\
+ \varepsilon[\Phi(\frac{+\varepsilon-\hat{g}_j(\boldsymbol{x}_{\text{un}})}{e_j(\boldsymbol{x}_{\text{un}})}) - \Phi(\frac{-\varepsilon-\hat{g}_j(\boldsymbol{x}_{\text{un}})}{e_j(\boldsymbol{x}_{\text{un}})})]
\end{aligned} \tag{4}
$$

Here, Φ refers to the cumulative density function of the normal distribution, while ϕ represents its probability density function. The parameter ε is a small constant factor proportional to e. By iteratively maximizing the EF function, the algorithm can effectively work on the exploration and exploitation of the constraint boundary during the optimizing procedure.

3. Proposed KMO-IR method

The flowchart of the proposed KMO-IR method is shown in Figure 2. The Latin Hypercube Sampling is used to generate an initial sample set. The open source ooDACE toolbox (Couckuyt et al. 2012) is used in this work to build Kriging models of objective and constraint functions. Based on the current Kriging models of constraints, the risks to be infeasible of current solutions caused by the input uncertainty are evaluated by the proposed IR formulation. Then, the Pareto solutions among the existing dataset are selected by non-dominated sorting. The corresponding PF will be an essential element in the infill searching stage. Guided by the proposed acquisition function, the modified EF (mEF), the KMO-IR algorithm will iteratively figure out the Pareto solutions with an improving convergency and diversity. The maximum computational resource is set as the termination criterion.

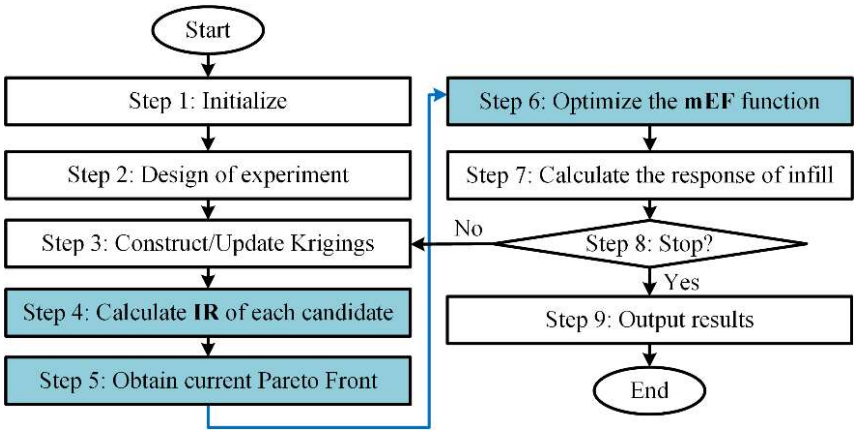

Figure 2. Flowchart of the proposed KMO-IR method.

In the following subsections, details of the developed IR formulation, the acquisition function mEF, and relative Hyper Area (rHA) will be presented.

3.1. Infeasibility Ratio formulation

When input uncertainty is present in constrained optimization problems, robustness is an important factor for determining feasibility, since the uncertainty may result in the fluctuations of constraint values. However, classifying candidate designs into 'feasible' and 'infeasible' groups may make the optimization overlook promising designs that are within tolerable risks caused by input uncertainty. In this subsection, the IR formulation is proposed and treated as an additional objective to flexibly deal with fluctuations of constraints.

A general constrained optimization problem under input uncertainty can be given as

$$\begin{aligned} &\min_{\boldsymbol{x}} \ \boldsymbol{f}(\tilde{\boldsymbol{x}})=\{f_1(\tilde{\boldsymbol{x}}), f_2(\tilde{\boldsymbol{x}}),..., f_M(\tilde{\boldsymbol{x}})\} \\ &\text{s.t. } \ \boldsymbol{g}(\tilde{\boldsymbol{x}})=\max(g_1(\tilde{\boldsymbol{x}}),g_2(\tilde{\boldsymbol{x}}),..., g_J(\tilde{\boldsymbol{x}}),0) \le 0 \\ &\tilde{\boldsymbol{x}} = \boldsymbol{x} + \Delta\boldsymbol{x}, \boldsymbol{x} \in [\boldsymbol{x}^{\mathrm{LB}}, \boldsymbol{x}^{\mathrm{UB}}], \Delta\boldsymbol{x} \sim \mathrm{N}(0, \sigma^2) \end{aligned} \tag{5}$$

Where $\Delta \boldsymbol{x}$ represents the input uncertainty, which is assumed to follow the Gaussian distribution N(0, σ^2). According to the 3-Sigma rule (McConaghy et al. 2013), we take

the range of $[+3\sigma, -3\sigma]$, as input uncertainty. Figure 3 illustrates the different scenarios resulting from input uncertainty.

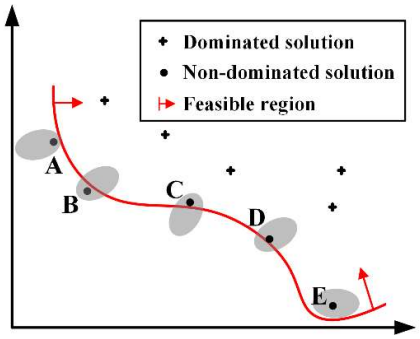

Figure 3. Illustration of different scenarios resulting from input uncertainty on the design solution. The grey area indicates the fluctuation of the design solution in the constraint space caused by input uncertainty.

For points A and E, the fluctuations of constraint do not cross the boundary, i.e., the uncertainty does not affect the final judgment of the feasibility of the design solution. For points B, C, and D, the feasibility status of the design solution may change due to the input uncertainty, especially if it is very close to the constraint boundaries. These candidates are categorized into the Partially-Feasibility (PaF) group. To assess the possibility of a design solution being infeasible given the input uncertainty, we propose an IR formulation as an additional optimization objective based on the 3-Sigma principle. During the optimization process, the original constraints are replaced by IR, formulated as

$$IR = \begin{cases} r - \alpha \sin(2\pi r), \text{ PaF} \\ 1, \ \bar{g} - 3\sigma > 0 \\ 0, \ \bar{g} + 3\sigma < 0 \end{cases} \quad (6)$$
$$where \ \ r = (\bar{g} + 3\sigma) / (6\sigma), \alpha \in (0.15, 0.2)$$

The $\bar{g}$ and σ are the nominal value and the corresponding variance, respectively, predicted by Kriging model of constraint. The α is an intensity factor to revise the ratio r of infeasible portion to 6-Sigma range. Figure 4 gives the illustration of the PaF group,

the infeasible portion caused by the input uncertainty, and the 6-Sigma range regarding the fluctuations of constraint.

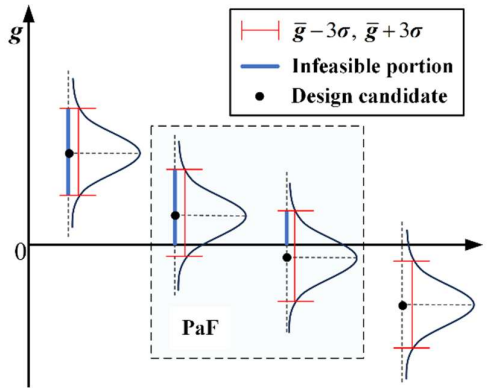

Figure 4. The Partially-Feasibility (PaF) solutions in constraint space.

By simultaneously optimizing the original objective and the additional IR objective, the constrained problem is converted into a multi-objective optimization problem. This approach ensures that the optimization algorithm focuses not only on feasible and globally optimal solutions but also on solutions near the constraint boundaries that are relatively sensitive to input uncertainty.

3.2. Modified Expected Feasibility

To deal with the constraints that exist in an optimization problem, the EF function is used to explore constraint boundaries and accurately predict feasibility. However, prioritizing only the solutions with feasibility robustness when the input uncertainty exists is inefficient and conservative. To simultaneously optimize the objective with full consideration of constrained input uncertainty and improve the quality of the PF, a modified Hypervolume Difference (mHD) is introduced to assist the update strategy of the sequential optimization procedure. Figure 5 illustrates the cases where the update point will affect the modified hypervolume (mHV) of the PF.

For each candidate $\boldsymbol{p}$, the algorithm performs a non-dominated sort to obtain the PF among the current sample set. The difference of mHV of the PF, corresponding to the

light-shaded region in Figure 5, compared to the previous iteration, can be formulated as

$$mHD=hv(\boldsymbol{S}_{pf} \cup \boldsymbol{p}) - hv(\boldsymbol{S}_{pf}) \tag{7}$$

where $\boldsymbol{S}_{pf}$ is the obtained PF in the previous iteration, and $hv(\boldsymbol{S}_{pf})$ is the mHV value of $\boldsymbol{S}_{pf}$. In early iterations, the algorithm usually fails to obtain the entire PF.

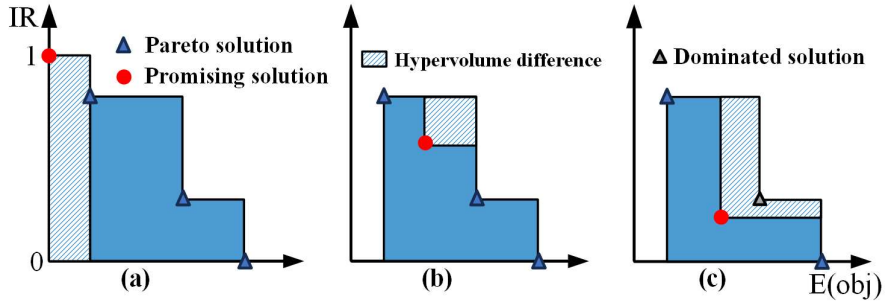

Figure 5. The possible situations for the mHD in a two-objective case. The red dot is the unknown candidate solution predicted by the Kriging model. mHD increases in (a) when the current PF is extended. In (b) and (c), the mHD decreases since the current PF is refined or the Pareto solution is dominated by adding the promising solution.

The improvement of the PF is measured by the absolute value of the hypervolume difference, which is given by

$$I_{hvpf} = \begin{cases} 0, \ \boldsymbol{p} \text{ is dominated by } \boldsymbol{S}_{pf} \\ abs\left(mHD\right), \text{otherwise} \end{cases} \tag{8}$$

If candidate $\boldsymbol{p}$ is dominated by the current PF, it will not influence the mHV of the PF. Hence, the proposed acquisition function modified Expected Feasibility (mEF) is formulated as

$$mEF = EF + \beta \cdot I_{hvpf} \tag{9}$$

The additive factor β is studied in Section 4.1 and a suggested value is given.

In sum, the original constrained optimization problem is transformed into a new unconstrained multi-objective optimization problem,

$$\begin{aligned}
&\min_{\boldsymbol{x}} \boldsymbol{f}(\tilde{\boldsymbol{x}}) = \{f_1(\tilde{\boldsymbol{x}}), f_2(\tilde{\boldsymbol{x}}), ..., f_M(\tilde{\boldsymbol{x}})\} \\
&\min_{\boldsymbol{x}} \boldsymbol{IR} = \max\{IR_j\}, j = 1, ..., J \\
&\text{s.t. } \tilde{\boldsymbol{x}} = \boldsymbol{x} + \Delta\boldsymbol{x}, \boldsymbol{x} \in [\boldsymbol{x}^{\text{LB}}, \boldsymbol{x}^{\text{UB}}], \Delta\boldsymbol{x} \sim \text{N}(0, \sigma^2)
\end{aligned} \tag{10}$$

In each iteration, the optimization problem is solved by maximizing the mEF function,

$$\boldsymbol{x}^* = \arg\max_{\boldsymbol{x} \in [\boldsymbol{x}^{\text{LB}}, \boldsymbol{x}^{\text{UB}}]} MEF(\tilde{\boldsymbol{x}} \mid \mathbf{K}_{mg}, \boldsymbol{S}_{pf}) \tag{11}$$

The $\mathbf{K}_{mg}$ indicates the Kriging models of objective and constraint functions.

3.3. Relative Hyper Area metric

Drawing inspiration from mHA, we developed a measure of the quality of PF under uncertainty. This relative Hyper Area (rHA) metric considers both refinement and extension of the PF as improvements, see Figure 6. Among all the obtained PFs, the augmented all-best and all-worst scenarios are obtained by slightly expanding the known best and worst values of each objective. By replacing the predefined reference points by augmented all-best and all-worst scenarios, the mHV is calculated, shown as the dark blue area in Figure 6. The HV formed by the augmented scheme that covers all PF solutions is referred to as the base Hypervolume (bHV). The ratio of PF's mHV to the bVH is its corresponding rHA value.

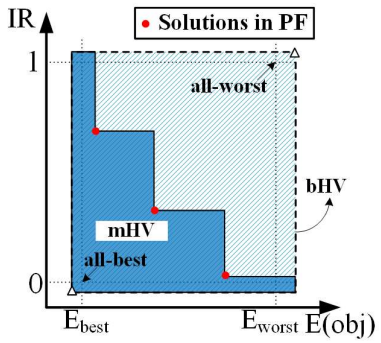

Figure 6. The schematic representation of rHA in a two-objective case. The two triangles represent the reference points corresponding to the augmented all-best and all-worst scenarios, respectively.

4. Numerical examples

Five numerical benchmark functions modified from Test-1D (TI), Branin (BR), Sasena A (SEA), Sasena B (SEB) and Gomez (GO) are employed to evaluate the performance of the proposed method (Chen, Liu, and Xu 2022; Forrester, Sobester, and Keane 2008; Dong et al. 2018; Wauters 2022). Details of all numerical cases can be found in Appendix Benchmarks. Each experiment is repeated 10 times.

4.1. Study of the parameters α and β

The parameter α should be set to an appropriate value in the IR formulation to provide an accurate approximation. The Test-1D (TI) and Sasena (SEA) functions are employed here to investigate the optimal value of α. The β is fixed at 0.5, while the value of α increases from 0.1 to 0.3. The mean absolute error (MAE) is used to indicate the predicted error of IR. Figure 7 illustrates the trend of MAE. The results of the analysis indicate that systematic bias occurs when α is less than 0.15 or greater than 0.2. In such cases, the IR formulation is at considerable risk of becoming invalid, and the algorithm may fail to converge to a meaningful PF. Therefore, the suggested range for α is $[0.15, 0.20]$.

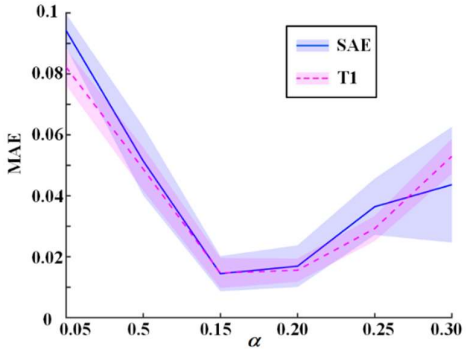

Figure 7. The Mean Absolute Error (MAE) for various settings of α.

To investigate the impact of the parameter β, the TI, SEA, and Gomez (GO) functions are solved using different values of β in the mEF. The rHA value and N_S,

representing the number of solutions in the Pareto set, are used as indicators to evaluate performance. The α is set to 0.20, while the β is varied to enable comparison analysis.

The trends of the indicators are depicted in Figure 8. It is not apparent that there are significant trends in performance under different values of β. From 0.75 to 1.25, the algorithm performance remains stable, consistently yielding PF with small rHA values and a moderate number of solutions. Therefore, the recommended range for β is 0.75 to 1.25. In this work, the predefined parameters are set as $\alpha = 0.2$ and $\beta = 1$.

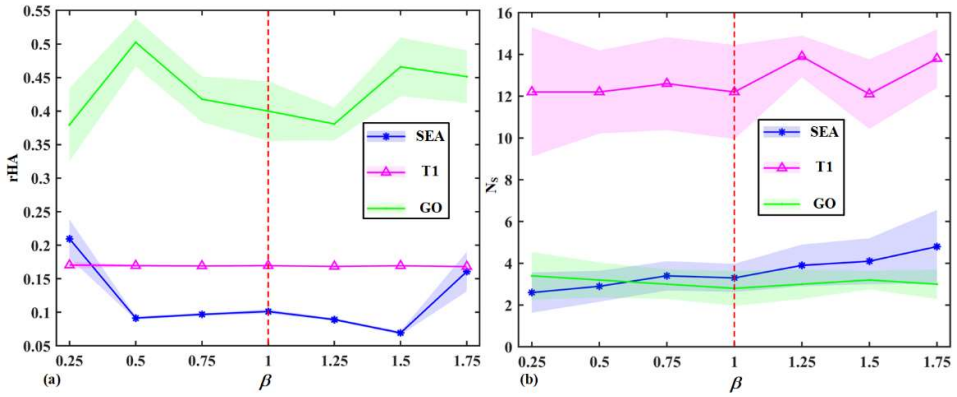

Figure 8. The rHA value and the number of solutions N_S for various settings of β.

4.2. Experimental setup

The parameter settings for the comparison methods EGO (Locatelli and Schoen 2021), ERGO (Wauters 2022), and ERGA (Bichon et al. 2008) are consistent with those of the proposed KMO-IR method to ensure fair comparison results. The IR is introduced into the comparison methods to conduct a comparison experiment. The MOGA (Maia et al. 2021) assisted by the Monte Carlo (MC) method (Zhang 2020), used to evaluate the IR of a certain solution, is adopted to solve numerical cases to obtain a baseline of the PF. Table 1 presents the parameters used for each method.

Table 1. The parameters and computational costs of methods under study.

method	Number of Initial samples	population	generation	Max number of infill points	Computational cost
EGO	11d-1	100	200	10×2^d	11d-1+10×2^d
ERGO	11d-1	100	200	10×2^d	11d-1+10×2^d
ERGA	11d-1	100	200	10×2^d	11d-1+10×2^d
KMO-IR	11d-1	100	200	10×2^d	11d-1+10×2^d
MOGA	/	100	200	/	$100\times200\times200$
KMOGA[a]	100d	100	200	/	100 d

[a]Only for the metamaterial vibration isolator.

The computational cost of each method is assessed in terms of the number of simulation calls. For numerical cases, the MOGA approach employs the MC method to generate 200 perturbations within the input uncertainty of each candidate to evaluate its IR. Since the finite-element simulation analysis is typically expensive and time-consuming, obtaining the baseline through the MOGA method with the MC technique is impractical. Hence, in the engineering application, a Kriging model based on 200 samples is introduced to assist the MOGA method in procuring an approximate baseline as a reference. In all other Kriging-assisted methods, the proposed IR formulation is introduced as an additional optimization objective.

4.3. Results and discussion

4.3.1. Illustrative example – Sasena (SEA) function

The SEA function is used to illustrate the algorithm process. Figure 9 shows the iterative results of the SEA function. In Figure 9(a), the current Kriging model cannot precisely give the boundary of feasible regions at iteration 5. The algorithm gives more priority to the unexplored areas near the boundary. In Figure 9(b), the locations of the updated points indicate that the algorithm searches the feasible boundary and the promising area

improving the PF of the MOO problem.

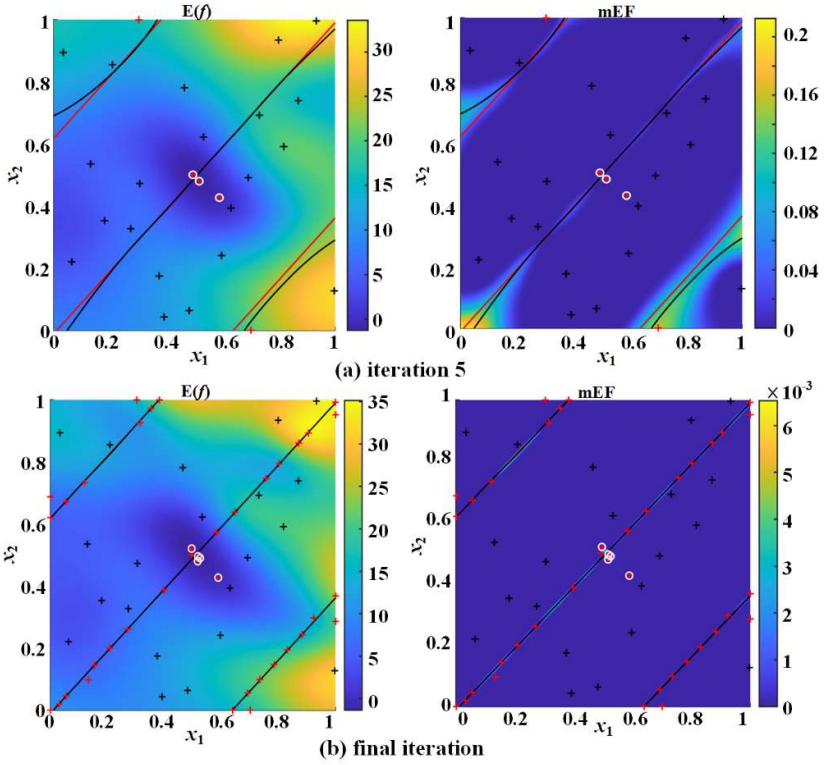

Figure 9. The iterative results of SEA function. The red and the black lines are the boundaries of the ground truth and predicted constraints, respectively. The black and the red crosses are the original and updated points for Kriging models. The white circles are solutions in PF at the current iteration.

To investigate the credibility of the obtained PF, 1000 perturbations around each solution are generated by the MC method to evaluate the actual IR caused by input uncertainty. The obtained PF is illustrated in Figure 10(a), and the verification result is shown in Figure 10(b). The verification result proves that the predicted IR is credible, and the KMO-IR can obtain multiple design solutions with different risks to be infeasible due to input uncertainty.

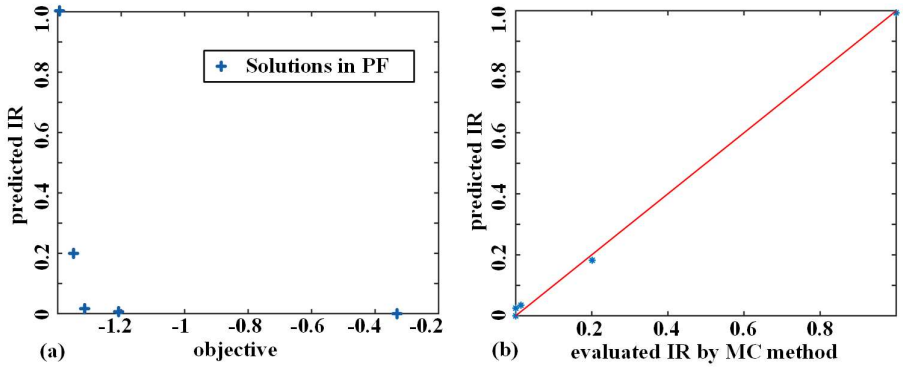

Figure 10. The obtained PF of SEA and the verification of predicted IR.

4.3.2. Comparison analysis

Table 2 lists the statistical results of rHA in the format 'mean±variance'. The proposed KMO-IR method can obtain a PF that closely resembles the baseline PF obtained from MOGA with much lower computational cost, whereas the PFs from the EGO, ERGO, and ERGA methods have higher rHA values. Meanwhile, the variances of rHA from KMO-IR are usually smaller than other methods, which means that the performance of the proposed method is stable. Figure A1 in Appendix 3 shows the PFs obtained by all methods in one experiment.

Table 2. The statistical results of rHA. MOGA row is a baseline for a reference. The optimal values are in bold.

	T1	BR	SEA	SEB	GO
EGO	0.230±0.001	0.126±5.2e-4	0.020±1.2e-6	0.718±0.012	0.362±0.021
ERGO	0.294±0.012	0.101±8.2e-4	0.021±2.5e-5	0.747±0.007	0.409±0.034
ERGA	0.256±0.006	0.215±0.014	0.272±0.023	0.682±0.004	0.259±0.002
KMO-IR	**0.176±5.8e-7**	**0.064±2.8e-7**	**0.019±2.0e-5**	**0.551±5.6e-6**	**0.216±9e-4**
MOGA	0.170±4.5e-7	0.056±1.7e-4	0.008±5.8e-8	0.547±2.1e-6	0.152±1e-6

The MC method is used to generate 1000 perturbations within the input uncertainty to conduct accuracy verification. Table 3 presents the MAE of the predicted

IR from different methods in each benchmark. All comparison methods and KMO-IR are with an acceptable prediction accuracy (minimum 97.95%). Compared to the MOGA method, the proposed KMO-IR method offers significant computational savings along with higher prediction accuracy for IR. In Table 3, the extremely low values of EGO, ERGO and ERGA in different benchmarks just indicate that these methods are too conservative to obtain diverse solutions with different IR levels. Furthermore, compared to the sequential EGO, ERGO, and ERGA methods, the KMO-IR method obtained PF with better rHA values, demonstrating its effectiveness and efficiency. In Appendix 3, the verification results for each benchmark are illustrated in Figure A2.

Table 3. The MAE of the predicted IR. MOGA row is a baseline for a reference. The highest values are in bold.

	T1	BR	SEA	SEB	GO
EGO	0.0182	8.6e-4	0.0102	0.0045	0.0054
ERGO	**0.0205**	0	0.0118	0.0038	**0.0170**
ERGA	0.0084	0.0032	0.0154	0.0032	0.0126
KMO-IR	0.0126	**0.0148**	**0.0178**	**0.0113**	0.0082
MOGA	0.0330	0.0504	0.0375	0.0192	0.0172

5. Engineering case: the design of a metamaterial vibration isolator with honeycomb structure

Undesirable vibrations can significantly impact the performance of the mechanical equipment and may shorten the service life. In mechanical engineering design, ensuring effective vibration isolation of the mechanical system is essential. Various vibration isolation strategies are developed to reduce harmful vibrations and inhibit the transmission of vibrations among mechanical systems (Mikhailov and Bazinenkov 2017; Al Rifaie, Abdulhadi, and Mian 2022). The metamaterial is highly competitive due to its

promising physical properties. The proposed KMO-IR method is applied to address the design of a metamaterial vibration isolator (Qian et al. 2021). Figure 11 illustrates the geometric structure of the metamaterial vibration isolator, comprising a polyurethane honeycomb structure with m=2 rows and n=4 columns of hexagonal honeycomb cells.

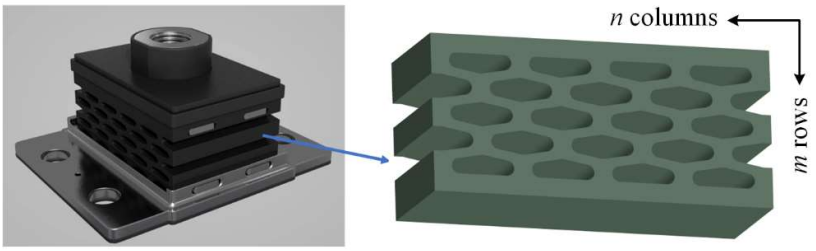

Figure 11. The geometry of the vibration isolator. (a) The CAD drawing; (b) the solid structure of the metamaterial vibration isolator.

5.1. Two-Dimensional design problem

The structure of the hexagonal honeycomb cell is illustrated in Figure 12. The cell is characterized by six geometric parameters: the length (L), the thickness (T_l), and the inclination angle (θ) of the oblique bar, the thickness (T_h) of the vertical bar, the radius (R_f) of rounding and the depth (D) of the cell. The L and T_h are two design variables. Information regarding geometric parameters is given in Table 4.

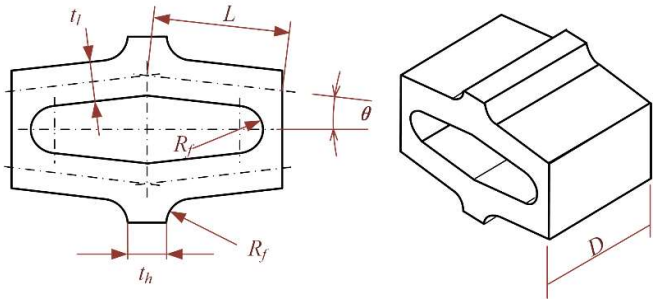

Figure 12. The geometric structure of the hexagonal honeycomb cell.

Table 4. The six geometric parameters of the hexagonal honeycomb cell. The design parameters are in bold.

Parameters	Values/Ranges	uncertainties
θ	10.3°	-
D	45mm	-
R_f	31mm	-
T_l	40mm	-
$\boldsymbol{L}$	**15.0~20.0mm**	$\mathbf{1\%}\times\boldsymbol{L}$
$\boldsymbol{T_h}$	**5.0~10.0mm**	$\mathbf{1\%}\times\boldsymbol{T_h}$

The optimization design problem of the metamaterial vibration isolator can be formulized as

$$\begin{aligned} &\min f_1 = \left|1-\frac{fre}{fre_0}\right|, fre_0 = 6\text{Hz} \\ &\min f_2 = \boldsymbol{IR} \\ &s.t.\ \ g_1 = 1-K_r/2.45 \le 0 \\ &\qquad g_2 = 1-\frac{\xi}{0.79} \le 0 \end{aligned} \tag{12}$$

The natural frequency *fre* under the rated load M=50kg is calculated as

$$fre = \frac{1}{2\pi}\sqrt{\frac{1.3k_s}{M}} \tag{13}$$

where k_s is the static stiffness. The goal is to optimize the structure to find a design solution that makes the natural frequency of the designed metamaterial vibration isolator as close as possible to the desired natural frequency fre_0=6Hz. One difficulty of the optimization design problem is that it is subject to two constraints. The first constraint requires the transverse-vertical stiffness ratio K_r to be no lower than 2.45. The other constraint lies in the nonlinear coefficient ξ, which must not be less than 0.79. Furthermore, the presence of input uncertainty in the design variables may compromise the feasibility of the design solution, or even make the design infeasible. Therefore, an additional objective is to provide the approximate IR for the specific design solution.

The natural frequency *fre*, transverse-vertical stiffness ratio K_r, and nonlinear

coefficient ξ can be determined through finite element simulation. Due to the linear stretching of the hexagonal honeycomb cell along the direction of depth, the finite element model can be constructed as a 2-D plane model and simulated by the ANSYS 2024 R2 software using the APDL. The finite element model is meshed with plane182 elements. Figure 13 gives an example of design L=15.3mm and T_h=6.4mm.

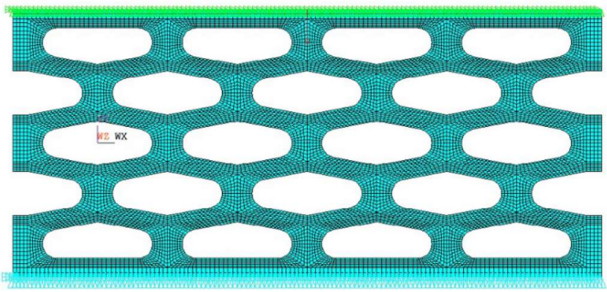

Figure 13. The finite element model of design L=15.3mm and T_h=6.4mm.

The objective and mEF response space predicted by the Kriging model is given in Figure 14. The white circles depict the final output solutions obtained by the proposed KMO-IR method. To investigate the accuracy of the predicted IR, all design solutions obtained from each method are verified. The PFs obtained from all methods and the verification results are shown in Figure 15.

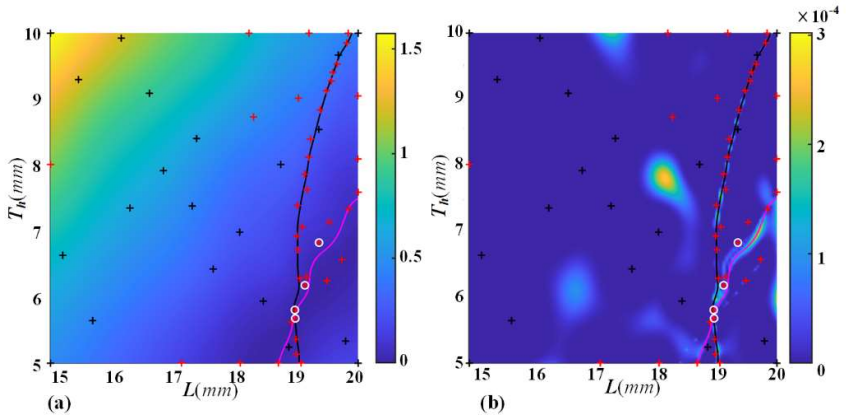

Figure 14. The predicted objective (a) and mEF (b) response space. The black and red crosses are the original and updated samples for Kriging. The black and magenta lines are the feasible boundaries of two constraints.

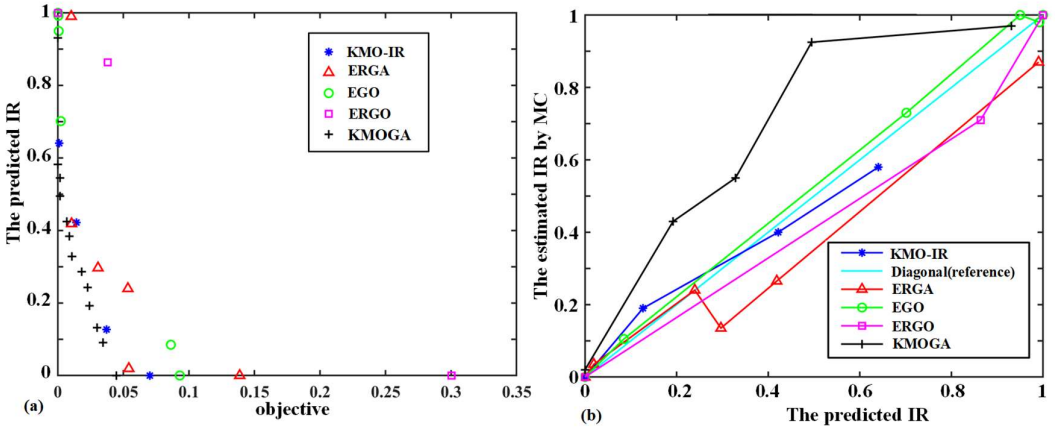

Figure 15. The PFs (a) from different methods and the verification results (b).

200 perturbations within the uncertainty around the nominal value are generated for each design solution and are simulated by a finite element model to evaluate their response values. (For the KMOGA method, only 30% are selected evenly from the PF solutions to avoid unnecessary time-consuming simulations.) The MAE of the predicted IR and statistical rHA of the PFs are collected in Table 5.

Table 5. The statistical results of rHA and MAE of the predicted IR. KMOGA row are separated for reference. The results from KMO-IR are in bold.

	rHA	MAE
EGO	0.177±0.0008	0.0184
ERGO	0.273±0.0439	0.0512
ERGA	0.111±0.0004	0.0753
KMO-IR	**0.095±7.59e-5**	**0.0364**
KMOGA	0.066±0.0003	0.1896

In this engineering case, the proposed KMO-IR method can save 69.5% computational costs compared to the KMOGA method, while also providing a more accurate estimate of IR for each design solution. The results obtained from KMOGA are meaningless due to the large MAE (0.1896). Compared to EGO, ERGO, and ERGA methods, the proposed KMO-IR method obtained a PF with the lowest rHA, indicating

its ability obtain a better PF. Additionally, the accuracy of predicted IR is 96.36%, which surpasses that of the ERGO and ERGA methods.

5.2. Three-Dimensional design problem

The design variables are given in Table 6, the experimental setup is the same as the two-dimensional problem version. The solutions obtained from different methods are shown in Figure 16.

Table 6. The input design variables of the 3-D case.

Variables	Ranges	Uncertainties
θ	5~10°	1%×θ
L	15.0~20.0mm	1%×L
T_h	5.0~10.0mm	1%×T_h

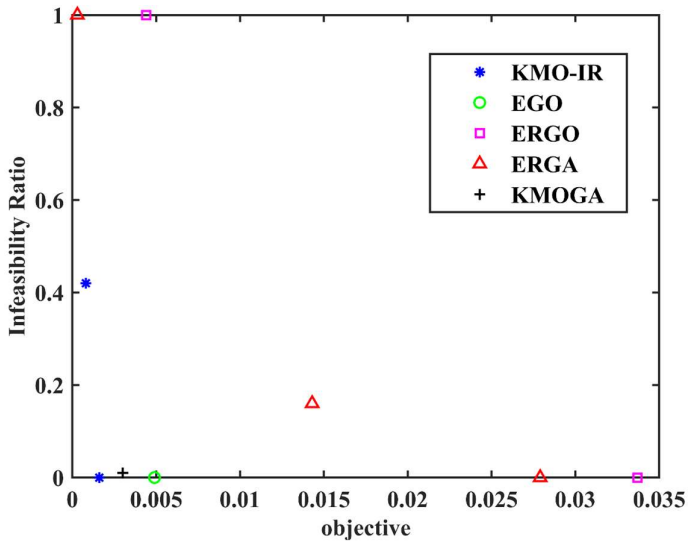

Figure 16. Pareto front of the different methods for the 3-D case.

The EGO and KMOGA methods outputted a single point with a low IR value while failing to obtain a PF which can trade off the feasibility robustness for better objective performance. The PFs from ERGO and ERGA methods are fully and partially dominated by the PF from the proposed method. For each solution, 100 perturbations are

generated by MC to evaluate the impact of input uncertainty and calculate the real IR. The rHA and MAE values are given in Table 7.

Table 7. The rHA of the PFs and the MAE of the predicted IR. The results from KMO-IR are in bold.

method	rHA	MAE
EGO	-	0
ERGO	0.1272	0
ERGA	0.0722	0.006
KMO-IR	**0.0087**	**0.018**
KMOGA	-	0.01

Since the outputs are single solutions, there is no rHA calculated for EGO and KMOGA methods. The proposed method obtained the PF with the best rHA value compared to the other PFs, which is consistent with what Figure 16 illustrates. The MAE of KMO-IR indicates the 98.2% accuracy of the predicted IR. In addition, compared to the KMOGA method, the proposed KMO-IR reduces 62.67% (1-(32+80)/300=62.67%) of the computational budget.

6. Conclusion

In this work, the KMO-IR method is proposed to address constrained optimization problems under input uncertainty. An IR formulation is developed and introduced as a constraint-handling technique. By treating IR as an additional optimization objective, KMO-IR aims to generate a Pareto set with diverse design solutions throughout the entire design space. Furthermore, an enhanced acquisition function, mEF, is proposed to guide the algorithm iteratively toward the locations with the most promising value for infill points. Based on the test results and comparison analysis, several conclusions can be drawn:

(1) The proposed KMO-IR method can obtain a Pareto set with multiple solutions and provide corresponding risks of infeasibility under input uncertainty. This offers designers multiple choices instead of only the safest solutions. The verification using the MC method demonstrates the effectiveness and accuracy of the IR approximation. (2) For the proposed KMO-IR, in numerical examples, the prediction accuracy of IR exceeds 98%; the accuracies are 96.36% and 98.2% for the 2-D and 3-D vibration isolator design problems, respectively. (3) In comparison to EGO, ERGO, and ERGA methods, the proposed KMO-IR method outperforms them as its obtained PFs exhibit the smallest rHA index. (4) the proposed KMO-IR method saves 99.9% and 69.5% (62.67% in the 3-D case) computational costs compared to MOGA and KMOGA methods, respectively.

For future research, we would like to explore the performance of the proposed method on more engineering applications as well as focus on improving the efficiency of the optimization algorithm.

Disclosure statement

No potential conflict of interest was reported by the authors.

Funding

This research receives funding from the Flemish Government under the "Onderzoeksprogramma Artifciele Intelligentie (AI) Vlaanderen" programme and the "Fonds Wetenschappelijk Onderzoek (FWO)" programme, and Chinese Scholarship Council (grant number 202106160005).

Appendix 1: Kriging

Given a sample set $\boldsymbol{S} = \{\boldsymbol{X}, \boldsymbol{Y}\}$ with N design points $\boldsymbol{X} = (\boldsymbol{x}_1, \boldsymbol{x}_2, \ldots, \boldsymbol{x}_n)$ and the corresponding function values $\boldsymbol{Y} = (y_1, y_2, \ldots, y_n)$, a Kriging model can be constructed.

And its general expression is given as

$$y(\boldsymbol{x}) = \mu(\boldsymbol{x}) + \tau(\boldsymbol{x}) \tag{14}$$

$\mu(\boldsymbol{x})$ is the regression part while $\tau(\boldsymbol{x})$ indicates the stochastic process, with a zero mean and σ^2 variance. The covariance function for any two points $\boldsymbol{x}_i$ and $\boldsymbol{x}_k$ is calculated as

$$\begin{aligned} &cov[\tau(\boldsymbol{x}_i), \tau(\boldsymbol{x}_k)] = \sigma^2 \boldsymbol{R}[r(\boldsymbol{x}_i, \boldsymbol{x}_k)] \\ &where \\ &r(\boldsymbol{x}_i, \boldsymbol{x}_k) = \exp\left[-\sum_{d=1}^{D} \theta_d \left| \boldsymbol{x}_i^d - \boldsymbol{x}_k^d \right|^2 \right] \end{aligned} \tag{15}$$

$\boldsymbol{R}$ is the correlation matrix infilled by the Gaussian correlation function $r(\boldsymbol{x}_i, \boldsymbol{x}_k)$. D represents the dimension of $\boldsymbol{x}$, and θ_d is the correlation parameter. By applying maximum likelihood estimation, the hyperparameters σ^2 and θ_d can be obtained for building the Kriging model.

For an unobserved design $\boldsymbol{x}_{\text{un}}$, the predicted response value $\hat{y}(\boldsymbol{x}_{\text{un}})$ and its variance $e^2(\boldsymbol{x}_{\text{un}})$ are represented as follows:

$$\hat{y}(\boldsymbol{x}_{\text{un}}) = \hat{\mu} + \boldsymbol{r}^T \boldsymbol{R}^{-1} (\boldsymbol{Y} - \boldsymbol{1}\hat{\mu}) \tag{16}$$

$$e^2(\boldsymbol{x}_{\text{un}}) = \sigma^2 \left[1 - \boldsymbol{1}^T \boldsymbol{R}^{-1} \boldsymbol{r} + \frac{(1 - \boldsymbol{1}^T \boldsymbol{R}^{-1} \boldsymbol{r})^2}{\boldsymbol{1}^T \boldsymbol{R}^{-1} \boldsymbol{1}} \right] \tag{17}$$

Where $\hat{\mu}$ is the estimated $\mu(\boldsymbol{x}_{\text{un}})$. The signal $\boldsymbol{r}$ indicates the correlation vector between $\boldsymbol{x}_{\text{un}}$ and N design points X. Vector 1 is an N-vector of ones.

Appendix 2: Benchmarks

- Test-1D function (T1)

$$\begin{aligned} &\min f_1 = (6x-2)^2 \sin(12x-4)/45 + 0.5 \\ &\min f_2 = IR \\ &s.t.\ \ g = (6x+1)^2 \sin(12x+10)/45 \\ &x = (\overline{x} + \Delta x), \overline{x} \in [0,1], \Delta x \sim \mathrm{N}(0, 0.01^2) \end{aligned} \tag{18}$$

- Branin function (BR)

$$\begin{aligned} &\min f_1 = \left(15x_2 - 5.1\left(15x_1 - 5\right)^2 / \left(4\pi^2\right) + 5\left(15x_1 - 5\right)/\pi - 6\right)^2 ... \\ &\qquad +10\left(\left(1 - 1/\left(8\pi\right)\right)\cos\left(15x_1 - 5\right) + 1\right) \\ &\min f_2 = IR \\ &s.t.\ \ g = -x_1 x_2 + 0.2 \\ &x_{1,2} = (\overline{x} + \Delta x), \overline{x} \in [0,1], \Delta x \sim \mathrm{N}(0, 0.01^2) \end{aligned} \tag{19}$$

- Sasena function A (SEA)

$$\begin{aligned} &\min f_1 = 2 + 0.01(5x_2 - (5x_1)^2)^2 + (1 - 5x_1)^2 + 2(2 - 5x_2)^2 ... \\ &\qquad +7\sin(2.5x_1)\sin(0.7 \times 5x_1 \times 5x_2) \\ &\min f_2 = IR \\ &s.t.\ \ g = -\sin\left(5x_1 - 5x_2 - \pi/64\right) \\ &x_{1,2} = (\overline{x} + \Delta x), \overline{x} \in [0,1], \Delta x \sim \mathrm{N}(0, 0.01^2) \end{aligned} \tag{20}$$

- Sasena function B (SEB)

$$\begin{aligned} &\min\ f_1 = -\left(x_1 - 1\right)^2 - \left(x_2 - 0.5\right)^2 \\ &\min\ f_2 = \boldsymbol{IR} \\ &\text{s.t.}\quad g_1 = \left(x_1 - 3\right)^2 + \left(x_2 + 2\right)^2 \exp\left(-x_2^7\right) - 12 \le 0 \\ &\qquad g_2 = 10x_1 + x_2 - 7 \le 0 \\ &\qquad g_3 = \left(x_1 - 0.5\right)^2 + \left(x_2 - 0.5\right)^2 - 0.2 \le 0 \\ &x_{1,2} = (\overline{x} + \Delta x), \overline{x} \in [0,1], \Delta x \sim \mathrm{N}(0, 0.01^2) \end{aligned} \tag{21}$$

- Gomez function (GO)

$$\begin{aligned} &\min f_1 = \left(4 - 2.1x_1^2 + \frac{1}{3}x_1^4\right)x_1^2 + x_1 x_2 + \left(-4 + 4x_2^2\right)x_2^2 \\ &\min f_2 = IR \\ &s.t.\ g(\boldsymbol{x}) = -\sin(4\pi x_1) + 2\sin^2(2\pi x_2) \le 0 \\ &x_1 = (\overline{x}_1 + \Delta x), \overline{x}_1 \in [-0.5, 0.5] \\ &x_2 = (\overline{x}_2 + \Delta x), \overline{x}_2 \in [-1, 0], \Delta x \sim \mathrm{N}(0, 0.01^2) \end{aligned} \tag{22}$$

Appendix 3: The illustrations of IR verification results.

The PFs obtained from all methods in one experiment are shown in Figure A1 and the results of verification for the IR are presented in Figure A2.

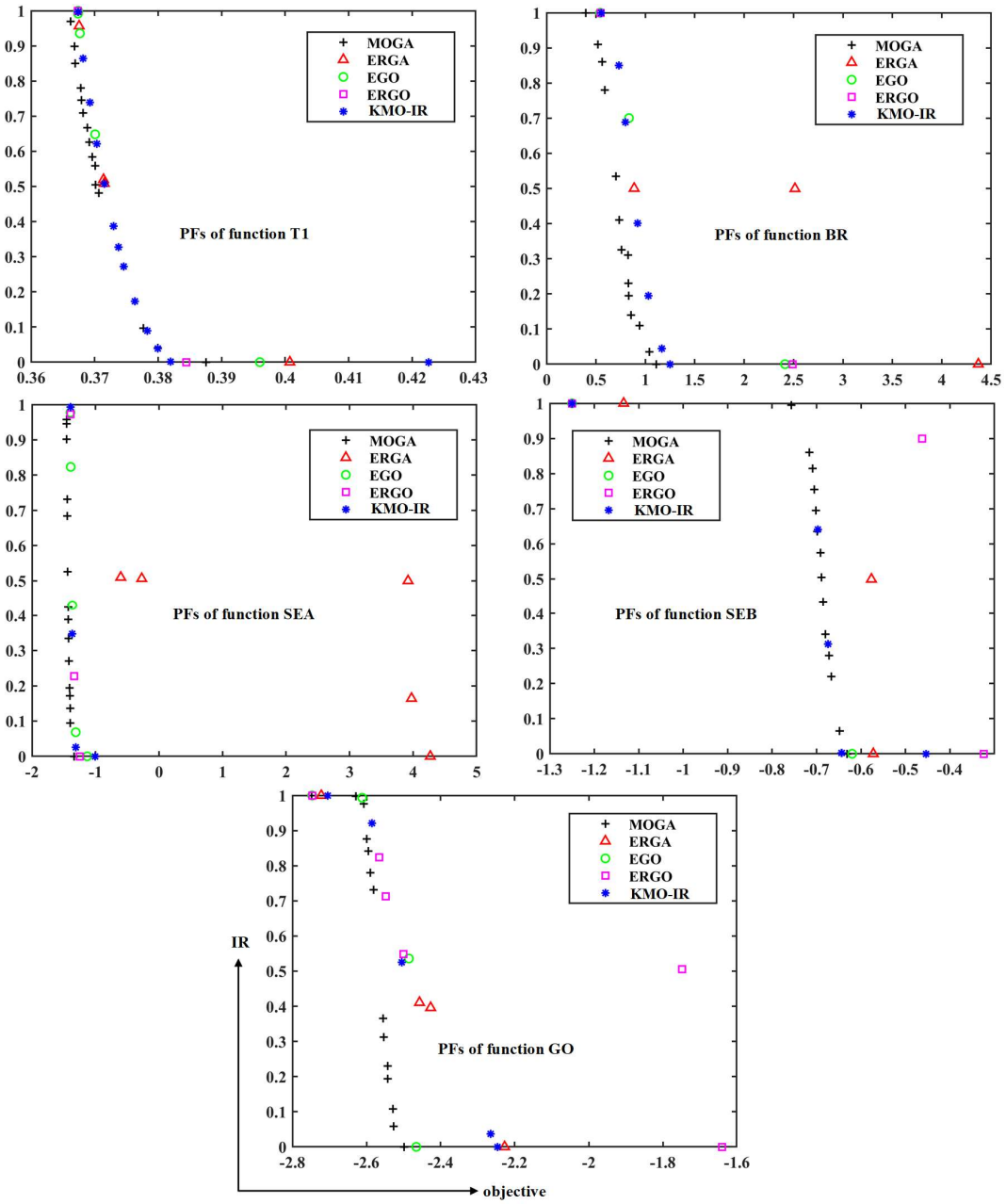

Figure A1. The illustration of PFs from all methods for each numerical case.

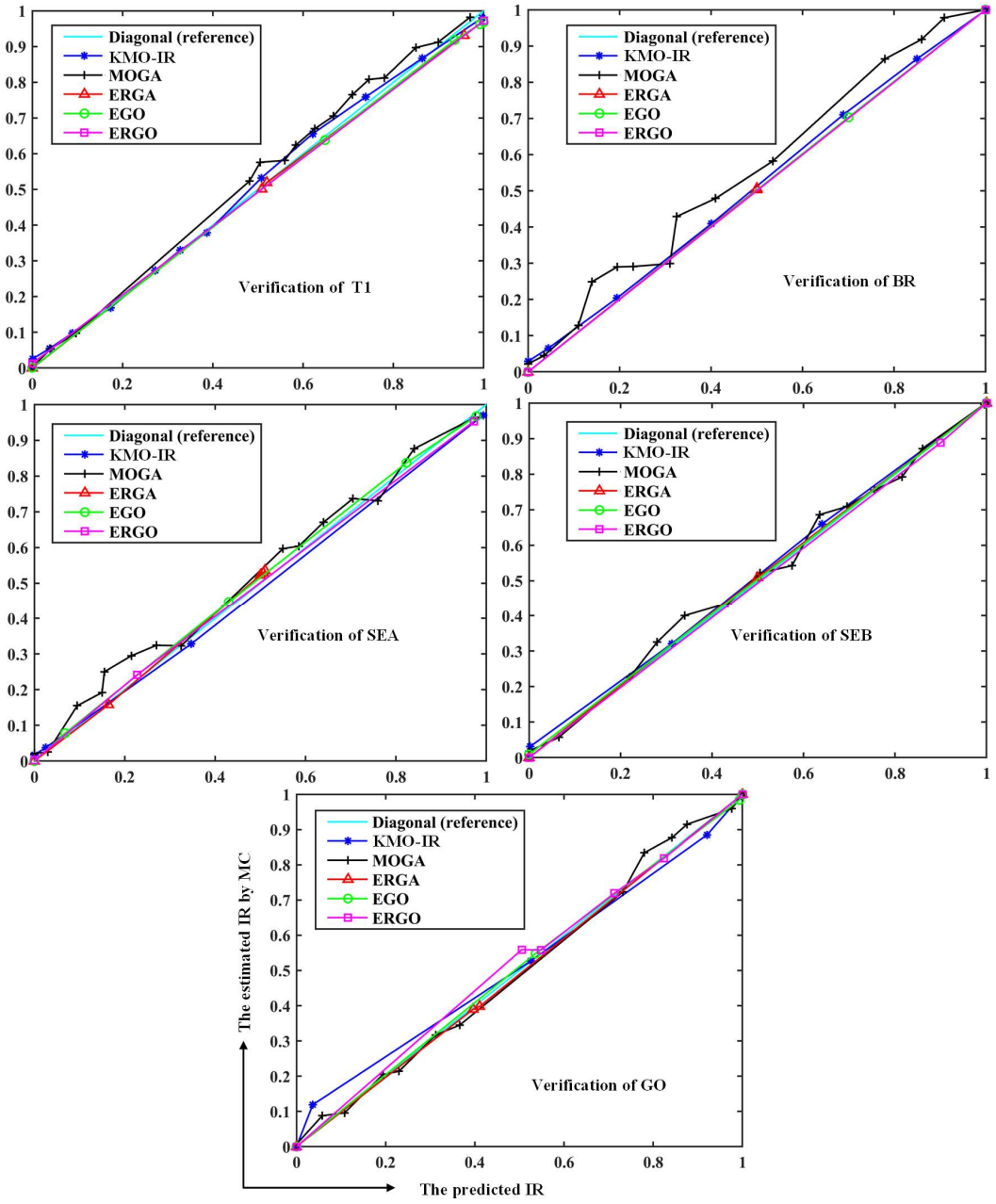

Figure A2. The illustrations of verification for each numerical case.

References

Al Rifaie, Mohammed, Hasanain Abdulhadi, and Ahsan Mian. 2022. "Advances in mechanical metamaterials for vibration isolation: A review." *Advances in Mechanical Engineering* 14 (3):45-64. https://doi.org/10.1177/16878132221082872.

Bichon, Barron J, Michael S Eldred, Laura Painton Swiler, Sandaran Mahadevan, and John McFarland. 2008. "Efficient global reliability analysis for nonlinear implicit performance functions." *AIAA journal* 46 (10):2459-2468. https://doi.org/10.2514/1.34321.

Chaudhuri, Anirban, Alexandre N Marques, and Karen Willcox. 2021. "mfEGRA: Multifidelity efficient global reliability analysis through active learning for failure boundary location." *Structural Multidisciplinary Optimization* 64 (2):797-811. https://doi.org/10.1007/s00158-021-02892-5.

Chen, Cong, Jiaxin Liu, and Pingfei Xu. 2022. "Comparison of parallel infill sampling criteria based on Kriging surrogate model." *Scientific Reports* 12:678. https://doi.org/10.1038/s41598-021-04553-5.

Cheng, Shuo, Jianhua Zhou, and Mian Li. 2015. "A new hybrid algorithm for multi-objective robust optimization with interval uncertainty." *Journal of Mechanical Design* 137 (2):021401. https://doi.org/10.1115/1.4029026.

Couckuyt, Ivo, A Forrester, Dirk Gorissen, Filip De Turck, and Tom Dhaene. 2012. "Blind Kriging: Implementation and performance analysis." *Advances in Engineering Software* 49:1-13. https://doi.org/10.1016/j.advengsoft.2012.03.002.

Dang, Qianlong, Wutao Shang, Zhengxin Huang, and Shuai Yang. 2025. "Constrained multi-objective optimization assisted by convergence and diversity auxiliary tasks." *Engineering Applications of Artificial Intelligence* 139 (A):109546. https://doi.org/10.1016/j.engappai.2024.109546.

de Winter, Roy, Bas van Stein, and Thomas Bäck. 2021. SAMO-COBRA: a fast surrogate assisted constrained multi-objective optimization algorithm. Paper presented at the International conference on evolutionary multi-criterion optimization.

Deb, Kalyanmoy, Amrit Pratap, Sameer Agarwal, and TAMT Meyarivan. 2002. "A fast and elitist multiobjective genetic algorithm: NSGA-II." *IEEE transactions on evolutionary computation* 6 (2):182-197. https://doi.org/10.1109/4235.996017.

Dong, Huachao, Baowei Song, Zuomin Dong, and Peng Wang. 2018. "SCGOSR: Surrogate-based constrained global optimization using space reduction." *Applied Soft Computing* 65:462-477. https://doi.org/10.1016/j.asoc.2018.01.041.

Forrester, Alexander, Andras Sobester, and Andy Keane. 2008. *Engineering design via surrogate modelling: a practical guide*: John Wiley & Sons.

Gunantara, Nyoman. 2018. "A review of multi-objective optimization: Methods and its applications." *Cogent Engineering* 5 (1):1502242. https://doi.org/10.1080/23311916.2018.1502242.

He, Chunlin, Yong Zhang, Dunwei Gong, and Xinfang Ji. 2023. "A review of surrogate-assisted evolutionary algorithms for expensive optimization problems." *Expert Systems with Applications* 217 (C):119495. https://doi.org/10.1016/j.eswa.2022.119495.

Jin, Yaochu, Handing Wang, Tinkle Chugh, Dan Guo, and Kaisa Miettinen. 2018. "Data-driven evolutionary optimization: An overview and case studies." *IEEE transactions on evolutionary computation* 23 (3):442-458. https://doi.org/10.1109/TEVC.2018.2869001.

Jin, Yin-Fu, Zhen-Yu Yin, Wan-Huan Zhou, and Hong-Wei Huang. 2019. "Multi-objective optimization-based updating of predictions during excavation." *Engineering Applications of Artificial Intelligence* 78:102-123. https://doi.org/10.1016/j.engappai.2018.11.002.

Jones, Donald R, Matthias Schonlau, and William Welch. 1998. "Efficient global optimization of expensive black-box functions." *Journal of Global Optimization* 13:455-492. https://doi.org/10.1023/A:1008306431147.

Juul-Nyholm, Herle Kjemtrup, and Tobias Eifler. 2023. "Multi-objective robustness indicators for evaluation and exploration of design margins." *Journal of Engineering Design* 35 (10):1227-1257. https://doi.org/10.1080/09544828.2023.2261336.

Kania, Randall J, and Shapour Azarm. 2023a. "Bi-Objective Surrogate Feasibility Robust Design Optimization Utilizing Expected Non-Dominated Improvement With Relaxation." *Journal of Mechanical Design* 145 (3):031703. https://doi.org/10.1115/1.4055738.

Kania, Randall J, and Shapour Azarm. 2023b. "Surrogate feasibility testing–cutting for single-objective robust optimization under interval uncertainty." *Engineering Optimization* 55 (6):964-980. https://doi.org/10.1080/0305215X.2022.2052287.

Kudva, Akshay, Wei-Ting Tang, and Joel A. Paulson. 2023. "Robust Bayesian optimization for flexibility analysis of expensive simulation-based models with rigorous uncertainty bounds." *Computers & Chemical Engineering* 181:108515. https://doi.org/10.1016/j.compchemeng.2023.108515.

Li, Jinglu, Huachao Dong, Peng Wang, Jiangtao Shen, and Dezhou Qin. 2023. "Multi-objective constrained black-box optimization algorithm based on feasible region localization and performance-improvement exploration." *Applied Soft Computing* 148:110874. https://doi.org/10.1016/j.asoc.2023.110874.

Li, Wei, Liang Gao, Akhil Garg, and Mi Xiao. 2022. "Multidisciplinary robust design optimization considering parameter and metamodeling uncertainties." *Engineering with Computers* 38:191–208. https://doi.org/10.1007/s00366-020-01046-3.

Lin, Quan, Anran Zheng, Jiexiang Hu, Leshi Shu, and Qi Zhou. 2023. "A multi-objective bayesian optimization approach based on variable-fidelity multi-output metamodeling." *Structural Multidisciplinary Optimization* 66 (5):100. https://doi.org/10.1007/s00158-023-03536-6.

Lin, Quan, Qi Zhou, Jiexiang Hu, Yuansheng Cheng, and Zhen Hu. 2022. "A sequential sampling approach for multi-fidelity surrogate modeling-based robust design optimization." *Journal of Mechanical Design* 144 (11):111703. https://doi.org/10.1115/1.4054939.

Liu, Bo, Vic Grout, and Anna Nikolaeva. 2017. "Efficient global optimization of actuator based on a surrogate model assisted hybrid algorithm." *IEEE Transactions on Industrial Electronics* 65 (7):5712-5721. https://doi.org/10.1109/TIE.2017.2782203.

Locatelli, Marco, and Fabio Schoen. 2021. "(Global) Optimization: Historical notes and recent developments." *EURO Journal on Computational Optimization* 9:100012. https://doi.org/10.1016/j.ejco.2021.100012.

Loka, Nasrulloh, Ivo Couckuyt, Federico Garbuglia, Domenico Spina, Inneke Van Nieuwenhuyse, and Tom Dhaene. 2023. "Bi-objective Bayesian optimization of engineering problems with cheap and expensive cost functions." *Engineering with Computers* 39 (3):1923-1933. https://doi.org/10.1007/s00366-021-01573-7.

Long, Wenyi, Huachao Dong, Peng Wang, Yan Huang, Jinglu Li, Xubo Yang, and Chongbo Fu. 2023. "A constrained multi-objective optimization algorithm using an efficient global diversity strategy." *Complex Intelligent Systems* 9 (2):1455-1478. https://doi.org/10.1007/s40747-022-00851-1.

Ma, Zhongwei, and Yong Wang. 2021. "Shift-based penalty for evolutionary constrained multiobjective optimization and its application." *IEEE Transactions on Cybernetics* 53 (1):18-30. https://doi.org/10.1109/TCYB.2021.3069814.

Maia, Adyson Magalhães, Yacine Ghamri-Doudane, Dario Vieira, and Miguel Franklin de Castro. 2021. "An improved multi-objective genetic algorithm with heuristic initialization for service placement and load distribution in edge computing." *Computer Networks* 194:108146. https://doi.org/10.1016/j.comnet.2021.108146.

McConaghy, Trent, Kristopher Breen, Jeffrey Dyck, Amit Gupta, Trent McConaghy, Kristopher Breen, Jeffrey Dyck, and Amit Gupta. 2013. "3-Sigma verification and design: rapid design iterations with Monte Carlo accuracy." *Variation-Aware Design of Custom Integrated Circuits: A Hands-on Field Guide: A Hands-on Field Guide*:65-114. https://doi.org/10.1007/978-1-4614-2269-3_4.

Mikhailov, Valery P, and Alexey M Bazinenkov. 2017. "Active vibration isolation platform on base of magnetorheological elastomers." *Journal of Magnetism Magnetic Materials* 431:266-268. https://doi.org/10.1016/j.jmmm.2016.10.007.

Price, C. J., and B. L. %J Operations Research Forum Robertson. 2024. "Using Estimated Gradients in Bound-Constrained Global Optimization." 6 (1).

Qian, Jiachang, Yuansheng Cheng, Anfu Zhang, Qi Zhou, and Jinlan Zhang. 2021. "Optimization design of metamaterial vibration isolator with honeycomb structure based on multi-fidelity surrogate model." *Structural Multidisciplinary Optimization* 64:423-439. https://doi.org/10.1007/s00158-021-02891-6.

Qing, Jixiang, Ivo Couckuyt, and Tom Dhaene. 2023. "A robust multi-objective Bayesian optimization framework considering input uncertainty." *Journal of Global Optimization* 86 (3):693-711. https://doi.org/10.1007/s10898-022-01262-9.

Shu, Leshi, Ping Jiang, Xinyu Shao, and Yan Wang. 2020. "A new multi-objective Bayesian optimization formulation with the acquisition function for convergence and diversity." *Journal of Mechanical Design* 142 (9):091703. https://doi.org/10.1115/1.4046508.

Song, Jingwen, Yifan Cui, Pengfei Wei, Marcos A Valdebenito, and Weihong Zhang. 2024. "Constrained Bayesian optimization algorithms for estimating design points in structural reliability analysis." *Reliability engineering system safety* 241:109613. https://doi.org/10.1016/j.ress.2023.109613.

Song, Zhenshou, Handing Wang, Cheng He, and Yaochu Jin. 2021. "A kriging-assisted two-archive evolutionary algorithm for expensive many-objective optimization." *IEEE transactions on evolutionary computation* 25 (6):1013-1027. https://doi.org/10.1109/TEVC.2021.3073648.

Song, Zhenshou, Handing Wang, Bing Xue, Mengjie Zhang, and Yaochu Jin. 2023. "Balancing objective optimization and constraint satisfaction in expensive constrained evolutionary multi-objective optimization." *IEEE transactions on evolutionary computation* 28 (5):1286-1300. https://doi.org/10.1109/TEVC.2023.3300181.

Wauters, Jolan. 2022. "ERGO: a new robust design optimization technique combining multi-objective bayesian optimization with analytical uncertainty quantification." *Journal of Mechanical Design* 144 (3):031702. https://doi.org/10.1115/1.4052009.

Wauters, Jolan. 2024. "ERGO-II: An Improved Bayesian Optimization Technique for Robust Design with Multiple Objectives, Failed Evaluations and Stochastic Parameters." *Journal of Mechanical Design* 146 (10):101704. https://doi.org/10.1115/1.4064674.

Wei, Hua, Leshi Shu, Yang Yang, Qi Zhou, Linjun Zhong, and Ping Jiang. 2021. "An improved sequential multi-objective robust optimisation approach considering interval uncertainty reduction under mixed uncertainties." *Journal of Engineering Design* 32 (2):61-89. https://doi.org/10.1080/09544828.2020.1858475.

Wei, Hua, Qi Zhou, Tom Dhaene, and Ivo Couckuyt. 2024. "Multi-objective constrained robust design of a metamaterial vibration isolator with a limited budget." *Journal of Engineering Design* 35 (3):241-262. https://doi.org/10.1080/09544828.2024.2306097.

Wu, Jin, and Shapour Azarm. 2001. "Metrics for quality assessment of a multiobjective design optimization solution set." *Journal of Mechanical Design* 123 (1):18-25. https://doi.org/10.1115/1.1329875.

Xie, Tingli, Ping Jiang, Qi Zhou, Leshi Shu, Yahui Zhang, Xiangzheng Meng, and Hua Wei. 2018. "Advanced multi-objective robust optimization under interval uncertainty using kriging model and support vector machine." *Journal of Computing Information Science in Engineering* 18 (4):041012. https://doi.org/10.1115/1.4040710.

Yi, Jiaxiang, Fangliang Wu, Qi Zhou, Yuansheng Cheng, Hao Ling, and Jun Liu. 2021. "An active-learning method based on multi-fidelity Kriging model for structural reliability analysis." *Structural Multidisciplinary Optimization* 63:173-195. https://doi.org/10.1007/s00158-020-02678-1.

Zhang, Jiaxin. 2020. "Modern Monte Carlo methods for efficient uncertainty quantification and propagation: A survey." *Wiley Interdisciplinary Reviews: Computational Statistics* 13 (5). https://doi.org/10.1002/wics.1539.

Zhang, Jize, and Alexandros A Taflanidis. 2019. "Multi-objective optimization for design under uncertainty problems through surrogate modeling in augmented input space." *Structural Multidisciplinary Optimization* 59:351-372. https://doi.org/10.1007/s00158-018-2069-1.

Zhong, Linjun, Yang Yang, Leshi Shu, Ping Jiang, and Hua Wei. 2022. "A surrogate model-assisted robustness-oriented tolerance design method based on 'reverse model'." *Journal of Engineering Design* 33 (7):491-516. https://doi.org/10.1080/09544828.2022.2106123.

Zhou, Jianzhao, and Jingzheng Ren. 2025. "Surrogate Modeling for Accelerating Optimization of Complex Systems in Chemical Engineering." In *Applied AI Techniques in the Process Industry*, 287-311.

Zhou, Qi, Jinhong Wu, Tao Xue, and Peng Jin. 2021. "A two-stage adaptive multi-fidelity surrogate model-assisted multi-objective genetic algorithm for computationally expensive problems." *Engineering with Computers* 37:623-639. https://doi.org/10.1007/s00366-019-00844-8.